Journal of Nanoparticle Research (2006) 8: 721–728
DOI 10.1007/s11051-006-9133-2


*Brief communication*

# Nanoparticle production using atmospheric pressure cold plasma

V. Vons[1,2,*], Y. Creyghton[2] and A. Schmidt-Ott[1]
[1]*Particle Technology, Delft University of Technology, Julianalaan 136, NL-2628 BL, Delft, The Netherlands;* [2]*TNO Defence, Security and Safety, P.O. Box 45 2280 AA, Rijswijk, The Netherlands; *Author for correspondence (Tel.: +31-015-2783540; Fax: +31-015-2784945; E-mail: v.a.vons@tudelft.nl)*

Received 16 March 2006; accepted in revised form 29 May 2006

*Key words:* nanoparticles, nanoparticle coating, generation, dielectric barrier discharge, atmospheric plasma

## Abstract

A new technique is proposed for the production and coating of nanoparticles, based on the dissociation of a volatile precursor in an atmospheric pressure, non-equilibrium (cold) plasma. The plasma is produced by a dielectric barrier discharge. Using this technique, nanoparticles were successfully produced from acetylene, ferrocene and hexamethyldisiloxane, using argon and helium as carrier gasses. Carbon nanoparticles were formed from acetylene when argon was used as a carrier gas, while in helium no particles were observed. The difference between the gasses is most likely due to the plasma structure. The argon plasma is filamentary, whereas in helium a homogeneous glow is observed. Using ferrocene, iron particles were produced, which rapidly oxidized to form iron oxide when exposed to ambient air. Preliminary experiments on particle coating suggest that coating by a silicon-based compound is possible.

## Introduction

In cold or non-equilibrium plasma, free electrons gain temperatures of several eV from the applied electric field, sufficient for ionisation and initiating chemical reactions, while ions and molecules (and thus the gas as a whole) remain at almost the initial temperature (Eliasson and Kogelschatz, 1991). When applied to nanoparticle production, the high-energy electrons present in the plasma interact with a volatile precursor, present in small concentrations in a suitable carrier gas. A metal organic complex is dissociated in this way, which results in a highly supersaturated metal vapour. Due to the low overall gas temperature, this vapour condenses to form nanoparticles. Hydrocarbons like methane or acetylene introduced into a plasma typically form chains and grow into higher hydrocarbons and polymers or polymer-like amorphous carbon (PAC), eventually forming particles (Kobayashi et al., 1974). The low process temperature prevents sintering of the created particles. Vollath and Szabó (1999) proved that after formation, the particles could be coated with a different compound in the same plasma system.

Vollath and Szabó (2005) have produced particles with very narrow size distributions using a cold microwave plasma. In contrast to other methods of producing nanoparticles from the gas phase, particle growth in plasmas seems to be governed by a growth-limiting effect, probably associated with the unipolar charge on particles incorporated in a dusty plasma. The cold plasma systems used so far have been low pressure (usually $< 40$ mbar) microwave and radio frequency plasmas. The low pressure requires a vacuum system, severely limits particle

production rates and makes on-line monitoring of particle production rather difficult.

Cold plasma at atmospheric pressure would make the process cheaper, easier to operate, capable of high production rates, and thus more readily applied to continuous production. Heating only the electrons and not the gas, a cold plasma process is inherently more economic concerning energy consumption. The narrow particle size distributions obtained by Vollath and Szabó (2005) under low pressure conditions as well as the feature of unipolar charge in the particle growth process are encouraging reasons for research in the direction of particle production in cold plasmas. Being equally charged, higher particle concentrations can, in principle, be maintained without coagulation, and combination with a cold plasma coating step directly downstream of particle formation could coat individual nanoparticles. At atmospheric pressure however, a plasma has the tendency to transform into a hot arc discharge, in which the gas temperature approaches the electron temperature, several thousands degrees Kelvin.

A dielectric barrier discharge (DBD) is a form of non-equilibrium plasma that can be operated at atmospheric pressure. It is generated by application of an oscillating electric field of sufficient strength to a gas flowing between two electrodes, *at least one of which is covered by a solid dielectric*. This dielectric barrier prevents the transition from cold non-equilibrium plasma to an equilibrium discharge (Kunhardt, 2000). Dielectric barrier discharges are widely used for chemical conversion; the primary industrial application being the large-scale production of ozone from air for water purification (Eliasson and Kogelschatz, 1991). Because of this, a lot of experience in scaling up of this technique already exists.

By using the right volatile precursors a myriad of different nanoparticles can be produced. These can be a metal organic precursors, available for a wide variety of metals, or silicon- or carbon compounds. In the present research, nanoparticle formation by atmospheric pressure dielectric barrier discharge was tested by producing carbon particles from acetylene ($C_2H_2$) and iron particles from ferrocene ($Fe(C_5H_5)_2$ or $FeCp_2$). Hexamethyldisiloxane (HMDSO, $(CH_3)_3SiO\text{-}Si(CH_3)_3$) and acetylene were applied to test the coating capability of the plasma source. Coating would, for example, provide protection against oxidation.

## Experimental

A schematic of the plasma source is depicted in Figure 1. Two concentric borosilicate glass tubes, with outer diameters of 20 and 26 mm and wall thicknesses of 2 mm, serve as the dielectric barriers. This leaves a 1-mm gap, between which the carrier gas and precursor(s) flow. A high voltage electrode (7 cm long) is situated inside the inner tube; a ground electrode (3 cm wide) surrounds the outer tube. A 76 kHz high voltage (2.8–4.8 kV rms) AC power source is used to generate the plasma. The visible length of the excitation zone varied between 3 and 8 cm, depending on carrier gas and applied voltage. Functionality for a second plasma stage with intermediate precursor addition was provided for to coat individual particles directly after formation.

Helium and argon were used as carrier gasses. Acetylene was introduced into the plasma by mass controlled flow, at 1–5 sccm. Ferrocene (Fluka, ≥ 98% purity) was introduced into the source by passing part of the carrier gas flow over approximately 30 g of ferrocene in a temperature-controlled container. The ferrocene concentration in the source was kept at 1, 2 or 6 ppm, with the vapour pressure given by the equation by Torres-Gomez et al. (1988). The plasma source was heated to 60°C on the outside by hot air in order to prevent ferrocene condensation. The gas temperature inside the plasma was estimated by measuring just behind the plasma, where the temperature varied between 80 and 120°C, depending on carrier gas and applied voltage. The total flowrate through the plasma source was kept at 5 l/min.

For coating experiments both plasma stages of the plasma source as depicted in Figure 1 were used. In the first stage, iron particles were made at 2 ppm $FeCp_2$ in argon. HMDSO for coating was

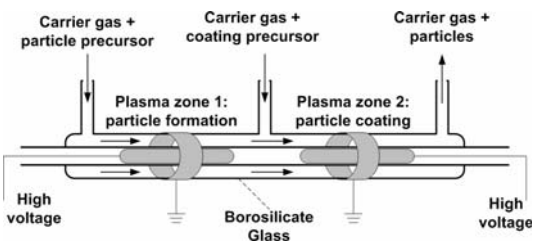


*Figure 1.* Schematic of the dielectric barrier plasma source. Arrows indicate gas flow.

added by bubbling part of the carrier gas through a bottle filled with HMDSO at room temperature. This stream was then introduced into the plasma source just behind the first plasma stage.

*Characterization*

Size distributions of produced particles were recorded using a differential mobility analyzer (DMA – TSI 3071) in conjunction with a particle counter, either a condensation particle counter (CPC – TSI 3025) or a faraday cup aerosol electrometer (AEM – produced in-house). Particles were charged using a Kr-85 radioactive bipolar charger. The particle size distribution is corrected for the equilibrium bipolar charging probability in argon according to Wiedensohler and Fissan (1991). No data is available on the equilibrium bipolar charge distribution in helium, and we restricted quantitative DMA measurements to argon.

Morphology and primary particle size of the carbon nanoparticles was determined using scanning electron microscopy (SEM). Iron-based nanoparticles were analysed using transmission electron microscopy (TEM). A Philips CM30T electron microscope, operated at 300 kV with a LaB6 filament as the source of electrons, was used. For the iron particles, energy dispersive X-ray spectra (EDX) were recorded using a LINK EDX system during the TEM analyses. Particle samples were collected for SEM and TEM by placing a TEM grid ~50 cm downstream of the plasma source, perpendicular to the gas flow and relying on diffusion. Nickel TEM grids were used (see Results and discussion section).

The results of coating experiments were also analyzed by TEM.

## Results and discussion

*Acetylene*

Large particle concentrations were detected with the DMA/CPC combination for 0.1–0.2 vol.% acetylene in both helium and argon carrier gas, regularly exceeding the maximum particle count ($10^5 cm^{-3}$) the CPC could handle. Particle size distributions for acetylene in argon were also recorded using the DMA/AEM combination. An example is given in Figure 2 (Argon, 0.1 vol.% $C_2H_2$). When helium was used as carrier gas no particles were seen on any SEM micrograph. For argon, large amounts of amorphous carbon particles and agglomerates, with a primary particle size of 30–50 nm were observed with SEM (Figure 3), partially embedded in a layer of carbonaceous material. Significant amounts of a yellowish coating were deposited inside and closely behind the plasma source. SEM analysis showed that it consists of a thick layer of carbon nanoparticles embedded in a type of 'matrix'. This matrix changes shape under influence of the electron beam and is therefore thought to consist of soft polymeric compounds. For helium, such deposition was not formed, but a thin layer with an oil-like sheen was observed.

Based on these results we speculate that polymerization of the acetylene in the helium plasma is not sufficient and only results in heavier hydrocarbons, not in solid particles; hydrocarbon droplets are then detected by the CPC but evaporate in the SEM. We suppose that even when argon is used as a carrier gas, only part of the acetylene is converted into carbon particles. The remaining acetylene most likely leaves the source unconverted or in the form of light hydrocarbons.

Depending on the conditions (gas type, voltage), an atmospheric pressure dielectric barrier discharge can be operated in a glow or filamentary mode. Glow plasmas are characterized by a very homogeneous structure throughout the discharge volume, with electron densities (at atmospheric pressure) typically at $10^{10}$–$10^{11} cm^{-3}$ (Kunhardt, 2000; Massines et al., 2003). In a filamentary discharge the non-uniform plasma is concentrated in

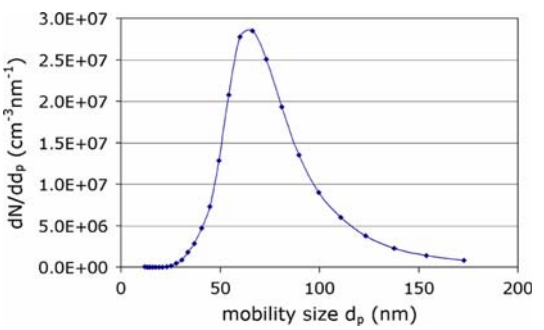


*Figure 2*. Particle size distribution of carbon particles formed from acetylene (0.1 vol. %) in an argon discharge.

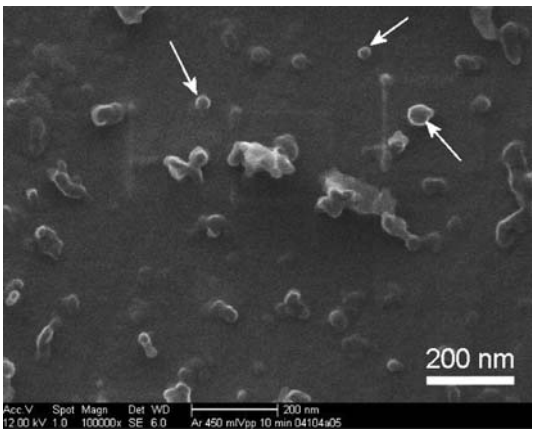


*Figure 3*. SEM micrograph of carbon particles formed in an argon discharge. Primary particles (arrows) and larger agglomerates (in the centre) are partially embedded in a carbonaceous film.

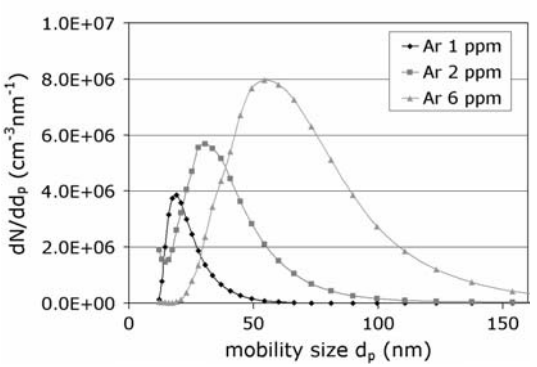


*Figure 4*. Particle size distributions as a function of ferrocene concentration.

a great number of small microdischarges or streamers, with a lifetime of 1–20 ns. Electron density in the streamers is typically $10^{14}$–$10^{15}$cm$^{-3}$ (Eliasson and Kogelschatz, 1991; Fridman and Kennedy, 2004). Based on the plasma current (Pashaie et al., 1999), the helium discharges were clearly of a glow-like nature, while the argon discharges are a mix of filamentary and glow. The difference in produced particles between argon and helium carrier gas is most likely due this difference in the plasma structure. The increased electron concentration in the filaments might be the key factor in inducing sufficient polymerization of the acetylene to form particles. These results are supported by the work of Jiang et al. (2001), who reported that film growth rate in an argon–acetylene filamentary DBD is much higher along the discharge filaments than elsewhere in the plasma, or in a glow discharge.

*Ferrocene*

A large number of particle size distributions were recorded by mobility analysis (DMA/AEM) for different process conditions. The count mean mobility diameter of the size distributions (CMMD) varied between 14 and 75 nm, depending mostly on the ferrocene concentration. This is demonstrated in Figure 4 for different ferrocene concentrations in argon.

Regardless of gas type, ferrocene concentration and whether or not hydrogen is added, TEM micrographs of deposited particles more or less all have the same general appearance as shown in Figure 5. The main difference between different process conditions is the amount of particles deposited. Very large agglomerates of nanoparticles are accompanied by strange wire structures, made up of straight particle strings. Evidently, the nickel grids are magnetized and lead to an alignment of magnetic particles. This is a convenient way of confirming the magnetic phase.

Considering the size of the agglomerates seen on the TEM grid and the particle size distributions recorded with the DMA/AEM, significant agglomeration takes place during deposition on the grid.

The EDX-spectrum of the micrograph shown in Figure 5 is presented in Figure 6. The nickel signal in the EDX spectra is due to background radiation hitting the nickel sample holder grid. The small silicon peak could point to a small amount of silicon being sputtered by the plasma from the borosilicate dielectric barriers. The presence of oxygen, the relatively high iron peak, and the absence of carbon indicate that the particles consist of iron and iron oxide. The darker areas inside the big agglomerates indicate pure iron, which has a high contrast in TEM. The lighter wire structures are assumed to be amorphous iron oxide. Particles are most likely pure iron when deposited on the grid in the inert atmosphere, and are oxidized when removed from the test set-up and exposed to air. The darker iron cores have most likely been protected from oxidation by the surrounding iron oxide.

Particle diameters of the iron oxide particles are between 6 and 11 nm. When an iron particle is

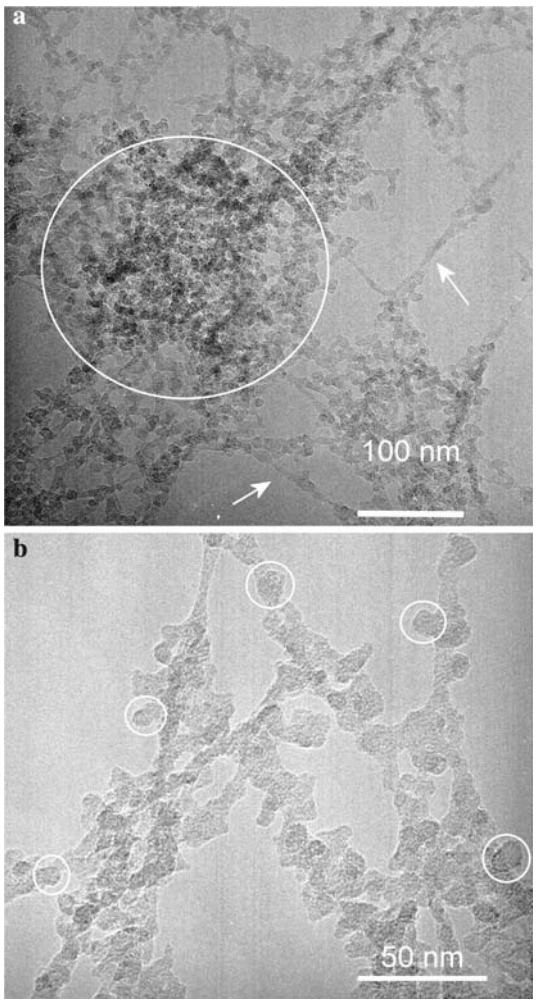


*Figure 5*. (a) TEM micrograph of the produced nanoparticles (91k× magnification). Note the large agglomeration of particles (indicated by circle), the darker areas deep inside this agglomeration, and the 'wires' stretching out from it (some indicated by arrows). Process conditions: 2 ppm $FeCp_2$ in helium, no hydrogen, 4.8 kV applied voltage. (b) TEM micrographs of the same sample at higher magnification (224k×). When an iron particle is oxidised, its diameter increases by ~30%, the resultant strain between adjacent particles can deform particles and make individual primary particles hard to discern. On the outer fringes of the wires particles are easier to distinguish (indicated by circles).

oxidised, its diameter increases by ~30%, the original iron particle primary size is therefore estimated to be 5–9 nm. Clearly the mobility size as recorded by the DMA is determined by agglomeration.

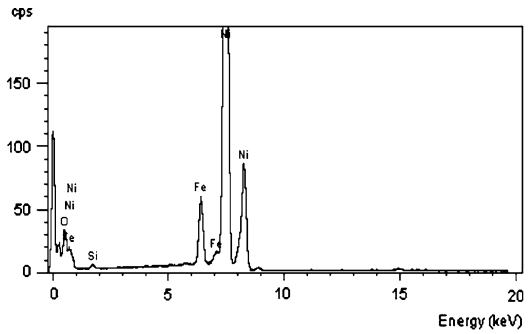


*Figure 6*. EDX spectrum of sample displayed in Figure 5. Process conditions: 2 ppm $FeCp_2$ in helium, no hydrogen, 4.8 kV applied voltage.

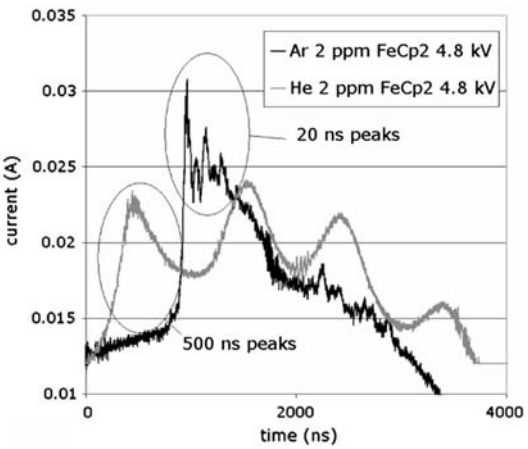


*Figure 7*. Current peak shape for ferrocene in both argon and helium. Note the smooth appearance of the helium line compared to argon.

Electron-impact studies (Müller and D'Or, 1967; Barfuss et al., 1987) indicate that iron atoms and ions and cyclopentadienyl radicals ($C_5H_5$ or Cp) are the dominant products of electron impact dissociation of ferrocene. The Cp radicals can result in carbon incorporation and/or formation of a separate carbon phase by decomposition or polymerization (Heszler et al., 2000; Ouchi et al., 2005). No carbon was detected with EDX, and no separate carbon phase is observed in the TEM micrographs. There may be a certain level of carbon incorporation into the particles below the EDX detection limit.

Working with ArF laser decomposition of ferrocene in argon, Heszler et al. (2000) produced particles consisting of an iron-rich core and a

separate surface layer of carbon. The difference between their results and this work is most likely due to the high temperature ($\geq$2600 K) their particles attain in the laser beam. This high temperature helps to decompose cyclopentadienyl radicals adsorbed on the surface of the iron nanoparticles. In our work particle temperature can be assumed equal to the gas temperature, which is close to room temperature. This follows from basic considerations on the temperature relaxation time at atmospheric pressure.

The discharge currents for both argon and helium discharges are given in Figure 7. In argon, a broad discharge current peak is observed, but current spikes of approximately 20 ns are superimposed. These spikes are associated with the short, random microdischarges of the filamentary regime. During the helium discharge, these current spikes are not observed. Current peaks in helium last approximately 500 ns, which is too long to be associated with microdischarges. Therefore the recorded discharge currents again indicate a glow plasma in helium, and a mix of filamentary and glow in argon.

The recorded particle size distributions also seem to indicate less agglomeration in argon, while the amount of particles is similar or even larger than in helium. We suppose that these two observations are closely related. A glow plasma becomes filamentary, when there is sufficient positive space charge build-up in the plasma, due to differences in mobility between electrons and positive ions (Fridman and Kennedy, 2004). The positive space charge in argon is larger, because the positive ions in argon are much less mobile than those in helium. Downstream of the excited zone, in the afterglow, there is rapid charge recombination of the mobile carriers (electrons and positive ions) and less rapid attachment of mobile carriers to particles. After recombination the excess positive charge remains and is reflected in the particle charge distribution observed. The dominance of the positive polarity on the particles produced in argon, explains the smaller degree of agglomeration in argon as compared to helium.

Removal of the bipolar charger and comparison of the concentrations with and without indicates that in argon, the positive particle concentrations amount to a significant fraction of the total, for some sizes exceeding 60%. This could significantly reduce agglomeration. In helium without bipolar charging, negative and positive particles occur with similar frequencies, with only a slight bias towards the positive polarity. The total amount of particles coming from the helium plasma cannot be determined due to the uncertainties surrounding the equilibrium bipolar charge distribution in helium.

Apart from this, there seems to be no big difference between the type and amount of particles formed in argon and helium, contrary to the results observed for acetylene. Most likely, conversion of the ferrocene is nearly complete for both carrier gasses, due to the relatively low electron energy required for dissociation. The consecutive splitting of two Cp radicals from ferrocene requires $\sim$4.0 eV ($FeCp_2$ in FeCp and Cp) and 2.2 eV (FeCp into Fe and Cp) (Barfuss et al., 1987).

The particle production rate of the current system is estimated to be between 1 and 10 mg/h. Dielectric barrier plasmas are also used on an industrial scale for ozone generators in water purifying plants. Here hundreds of plasma tubes are operated in parallel to achieve sufficient production rates. The same could be done to increase the nanoparticle production rate. Optimization of the process parameters is expected to further improve production rates.

*Hexamethyldisiloxane*

Particle size distributions were recorded to see if the plasma can form particles from HMDSO alone, before attempting to coat particles from ferrocene with this precursor. An example of these size distributions is given in Figure 8, for 145 ppm HMDSO in argon, at different voltages. For comparable production rates, the required HMDSO concentration is clearly much higher than that of ferrocene. The particle production rate is strongly dependent on the applied peak-to-peak voltage, much more so than with ferrocene.

The higher required HMDSO concentration is attributed to the fact that only a part of the introduced HMDSO polymerizes to long enough chains to form particles, similar to acetylene. Previous investigations in the behaviour of HMDSO in (low pressure) plasmas suggest a polymerization mechanism (Alexander et al., 1997), initiated by the $(CH_3)_3SiOSi^+(CH_3)_2$ ion, which has an appearance energy of $\sim$9.6 eV, much

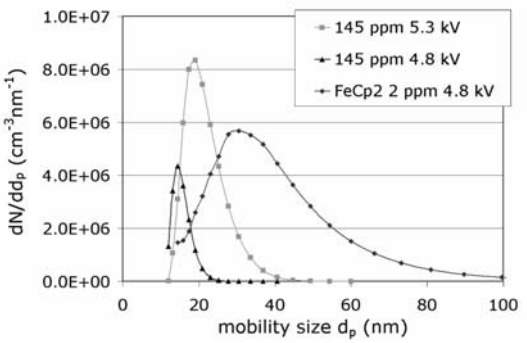


*Figure 8*. Particle size distributions for HMDSO in Ar at different voltages. The particle size distribution for 2 ppm ferrocene in Argon is added for comparison.

higher than the dissociation energies for ferrocene. Since the reaction is far from complete, this could explain the stronger dependence of HMDSO particle formation on plasma voltage, as a higher voltage will result in more electrons with sufficient energy to ionize a HMDSO molecule.

*Coating*

A TEM micrograph showing the result of one of the coating experiments, conducted with HMDSO and iron particles made at 2 ppm $FeCp_2$ in argon, is shown in Figure 9. As in the uncoated case (Figure 5), we see light grey wire structures associated with iron oxide nanoparticles and darker regions, again on the inside of agglomerates. This

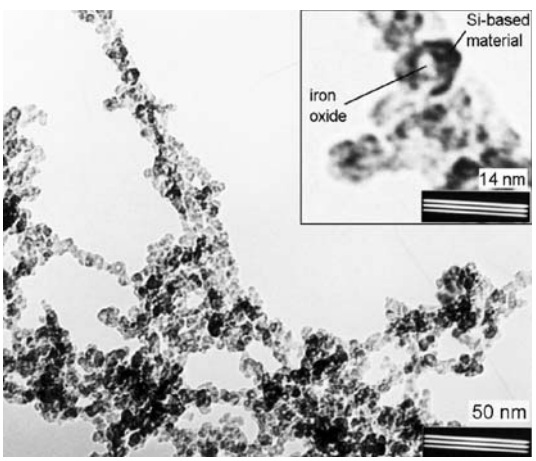


*Figure 9*. TEM micrograph of the result of a coating experiment.

indicates that the object of the coating, protection of iron particles from oxidation, is not achieved, at least not completely.

Closer analysis of dark particles at the *outside* of agglomerates revealed that these contain a much higher portion of silicon than the rest of the sample and thus consist of the coating material. In some cases, they cover the iron oxide nanoparticles, as indicated in the insert of Figure 9. This suggests that coating of single primary particles or small clusters has taken place. A slight trembling motion of the non-conducting particles in the electron beam hindered higher resolution micrographs. In most cases the silicon containing regions are separated from the lighter iron oxide, indicating homogeneous instead of heterogeneous nucleation of the silicon-based material.

Upon closer analysis of the appearance of the plasma, colour gradients were seen, indicating inhomogeneity. Thus, there was hardly any mixing between the gas stream containing the iron particles and that containing the coating precursor before the second plasma stage. This explained the limited amount of coating events, as these were restricted to the boundary layer between these gas streams. A redesign of the plasma source is needed to achieve proper turbulent mixing.

The particle size distributions recorded with the DMA indicate that the particles are quite strongly agglomerated when compared to the primary particle sizes on the micrographs. This is because the DMA had to be placed much further downstream of the plasma source than the coating stage due to the plasma source heating and power equipment. By the time particles reach the DMA they have had significant time for agglomeration, whereas for the coating stage the time for agglomeration is very limited.

We believe that the new approach introduced here will enable coating of *individual* particles like Vollath and Szabó (2005) have shown this under low pressure conditions. They state that the particles are positively charged in the plasma and that Coulomb forces keep them separated. In the case of Ar, much of this positive charge was retained downstream of our plasma. Placing the coating zone closer to the first plasma, or even stretching the plasma zone and introducing the coating precursor in the middle should lead to similarly successful coating of individual particles as in the case of Vollath and Szabó (2005).

## Conclusion

Using an atmospheric pressure non-equilibrium plasma based on dielectric barrier technology, nanoparticles were successfully produced from acetylene and ferrocene. Particles were characterised by mobility particle sizing and electron microscopy. For acetylene, carbon nanoparticles were formed when argon was used as a carrier gas, in helium no particles were observed. This difference is most likely due to the difference in plasma structure observed for these two gasses. In argon, the plasma is of a filamentary nature, while in helium a homogeneous glow is observed.

Using ferrocene, iron particles were produced, which rapidly oxidized to form iron oxide when exposed to ambient air. Although no significant difference in the amount and type of particles produced was observed between argon and helium, agglomeration of primary particles was less pronounced in argon. We propose that again the plasma structure, which strongly influences particle charge, is the cause of this difference.

Hexamethyldisiloxane was used to attempt to coat iron particles with a silicon-based compound. Our results strongly suggest that some of the particles were indeed coated, while most of the HMDSO nucleated homogenously. We conclude that there is a mixing zone, where the conditions lead to coating. The present reactor evidently does not introduce enough turbulence to obtain fast and homogeneous mixing with the coating precursor. It does suggest the feasibility of a combined nanoparticle production and coating process based on a dielectric barrier discharge at normal pressure.

## Acknowledgement

This project was supported by the Delft Institute of Sustainable Energy. We thank U. Lafont of the National Centre for High Resolution Electron Microscopy for preparing the electron micrographs and EDX spectra.

## References

Alexander M.R., F.R. Jones & R.D. Short, 1997. Mass spectral investigation of the radio-frequency plasma deposition of Hexamethyldisiloxane. J. Phys. Chem. B 101, 3614–3619.

Barfuss S., M. Grade, W. Hirschwald, W. Rosinger, N.M. Boag, D.C. Driscoll & P.A. Dowben, 1987. The stability and decomposition of gaseous chloroferrocenes. J. Vac. Sci. Technol. A 5, 1451–1455.

Eliasson B. & U. Kogelschatz, 1991. Nonequilibrium volume plasma chemical processing. IEEE Trans. Plasma. Sci. 19, 1063–1077.

Fridman A. & L.A. Kennedy, 2004. Plasma Physics and Engineering. New York: Taylor & Francis.

Heszler P., K. Elihn, M. Boman & J.-O. Carlsson, 2000. Optical characterisation of the photolytic decomposition of ferrocene into nanoparticles. Appl. Phys. A 70, 613–616.

Jiang N., S.F. Qian, L. Wang & H.X. Zhang, 2001. Localized material growth by a dielectric barrier discharge. Thin Solid Films 390, 119–122.

Kobayashi H., A.T. Bell & M. Shen, 1974. Plasma polymerisation of saturated and unsaturated hydrocarbons. Macromolecules 7(3), 277–283.

Kunhardt E.E., 2000. Generation of large volume, atmospheric pressure, non-equilibrium plasmas. IEEE Trans. Plasma Sci. 28, 189–200.

Massines F., P. Segur, N. Gherardi, C. Khampan & A. Ricard, 2003. Physics and chemistry in a glow dielectric barrier discharge at atmospheric pressure: Diagnostics and modelling. Surf. Coat. Technol. 174–175, 8–14.

Müller J. & L. D'Or, 1967. Massenspektrometrische untersuchungen an dicyclopentadienylcomplexen von übergangsmetallen. J. Organometal. Chem. 10, 313–322 (article in German).

Ouchi A., T. Tsunoda, Z. Bastl, M. Maryško, V. Vorlíček, J. Boháček, K. Vacek & J. Pola, 2005. Solution photolysis of ferrocene into Fe-based nanoparticles. J. Photochem. Photobiol. A: Chem. 171, 251–256.

Pashaie B., R. Sankaranarayanan & S.K. Dhali, 1999. Experimental investigation of microdischarges in a dielectric-barrier discharge. IEEE Trans. Plasma Sci. 27(1), 22–23.

Torres-Gómez L.A., G. Barreiro-Rodríguez & F. Méndez-Ruíz, 1988. Vapour pressures and enthalpies of sublimation of ferrocene, cobaltocene and nickelocene. Thermochim. Acta 124, 179–183.

Vollath D. & D.V. Szabó, 1999. Coated nanoparticles: A new way to improved nanocomposites. J. Nanoparticle Res. 1, 235–242.

Vollath D. & D.V. Szabó, 2005. The Microwave plasma process – a versatile process to synthesize nanoparticulate materials. J. Nanoparticle Res., 8, 417–428.

Wiedensohler A. & H.J. Fissan, 1991. Bipolar charge distributions of aerosol particles in high purity argon and nitrogen. Aerosol Sci. Technol. 14, 358–364.